

1 **Proof**

*Analytical &  
Bioanalytical  
Electrochemistry*

2025 by CEE  
[www.abechem.com](http://www.abechem.com)

---

7 *Full Paper*

8 **Beyond Randles-Sevcik Formalism: Towards**  
9 **Understanding Peak Currents of Nernstian Redox**  
10 **Systems in Square-Wave Voltammetry**

11 **Milkica Janeva, Pavlinka Kokoskarova, and Rubin Gulaboski\***

12 *Faculty of Medical Sciences, Goce Delcev University, Stip, Macedonia*

13 \*Corresponding Author, Tel.: +38975331078

14 E-Mail: [rubin.gulaboski@ugd.edu.mk](mailto:rubin.gulaboski@ugd.edu.mk)

15 *Received: 7 July 2025 / Received in revised form: 16 September 2025 /*

16 *Accepted: 28 September 2025 / Published online: 31 December 2025*

---

17 **Abstract-** In redox systems that obey the Nernst equation, where the surface and bulk  
18 concentrations remain in equilibrium during the potential sweep, the Randles-Sevcik equation  
19 is seen as a standard tool in both fundamental and applied linear scan voltammetry. As the  
20 Randles-Sevcik equation is seen as a key theoretical framework for interpreting voltammetric  
21 behavior in electrochemically reversible and diffusion-controlled redox systems considered  
22 under conditions of linear scan voltammetry, this foundational relationship becomes  
23 inapplicable when extended to pulse voltammetric techniques. Pulse voltammetric techniques  
24 differ fundamentally from linear scan voltammetric methods in both potential modulation and  
25 in current measurement protocols. The form of applied bias in pulse voltammetric techniques  
26 leads to conditions in which each applied pulse disrupts the diffusion profile of redox species  
27 of interest. Repeated disruption and compression of diffusion profiles in pulse voltammetric  
28 techniques introduce significant complexity into the current-potential behavior of redox  
29 species, thereby precluding the direct application of the Randles-Sevcik formalism. This study  
30 presents some basic theoretical insights into the limitations of applying Randles–Sevcik-type  
31 equations to square-wave voltammetry. In addition, a unifying parameter has been identified  
32 that governs the peak current response in square-wave voltammetry, which integrates the  
33 effects of potential step, frequency, square-wave amplitude, and temperature. At constant  
34 magnitude of the diffusion coefficient, this critical parameter is defined as  $\chi = constant \cdot$   
35  $(F/RT) \cdot [E_{sw}/(dE \cdot f)]^{1/2}$  and it is seen as a foundation for developing more comprehensive models  
36 and analytical expressions describing peak current dependencies under square-wave  
37 voltammetric conditions.  
38

39 **Keywords-** Randles-Sevcik equation; Square-wave voltammetry; Square-wave amplitude;  
40 peak currents in pulse techniques; Concentration gradients

---

## 1 1. INTRODUCTION

2 Voltammetric methods are widely recognized as some of the fastest, most cost-effective,  
3 and most efficient tools designed for investigating the mechanistic, kinetic, and thermodynamic  
4 aspects of various redox systems [1-3]. Owing mainly to its simplicity, sensitivity, and robust  
5 diagnostic capabilities, the cyclic voltammetry (CV) stands out as one of the most extensively  
6 employed among the other electrochemical techniques [3]. Major advantages of CV arise from  
7 its distinctive operational protocols and the easiness in interpretability the resulting  
8 voltammetric outputs. The fundamental principles of cyclic voltammetric theory provide a  
9 clear and systematic basis for interpreting complex electrochemical mechanisms, while also  
10 offering a very practical framework for kinetic measurements and analytical applications.  
11 Among the foundational concepts in the analysis of data obtained by conventional linear scan  
12 cyclic voltammetry stays the so-called "Randles-Sevcik equation" [2-6]. As it quantitatively  
13 relates the magnitudes of peak currents to the key parameters governing diffusion-controlled  
14 reversible electrode reactions, this equation represents a cornerstone in mechanistic  
15 investigations, analytical determinations, and in evaluation of diffusion coefficients of redox  
16 species of interest. The Randles-Sevcik equation is particularly applicable in linear scan  
17 voltammetry for electrochemical systems exhibiting Nernstian behavior, implying that the  
18 electrode reaction remains reversible and maintains near-equilibrium conditions throughout  
19 entire potential sweep. The Randles-Sevcik equation establishes a simple relationship between  
20 the magnitude of measured peak current ( $I_p$ ) and several key parameters, including the analyte's  
21 of interest bulk concentration, applied scan rate, temperature, and the diffusion coefficients of  
22 redox active forms [4-7]. Generally speaking, this equation makes a direct correlation between  
23 the magnitude of the measured voltammetric peak currents and the mass transport properties  
24 of electroactive redox species that are dissolved in solution. At 25°C (298 K), for  
25 electrochemically reversible electrode reaction in which electrons are exchanged in one-step,  
26 this equation can be written in following well-known form [2-4,7]:

$$27 \quad I_p = 2.69 \times 10^5 n^{3/2} D^{1/2} A c^* \nu^{1/2} \quad (1)$$

28 In equation (1) " $n$ " stays for the number of electrons transferred, " $A$ " stays for the active  
29 area of working electrode, " $D$ " is the diffusion coefficient of the molecules/ions of redox active  
30 species of interest, " $c^*$ " is the bulk molar concentration of the redox analyte of interest, while  
31 " $\nu$ " is the applied scan rate. The square-root dependence of the peak current on applied scan  
32 rate ( $\nu$ ) and on the diffusion coefficient makes this equation a basis for determining diffusion  
33 coefficients of electroactive species of interest, but it is also suitable for assessing the  
34 electrochemical reversibility of electron transfer processes. Its relevance extends to studies of  
35 biological redox centers of water-soluble enzymes, water-soluble coordination complexes,  
36 battery materials, in biosensors design, and many more [1-4].

1        Although the Randles-Sevcik equation serves as a fundamental analytical tool in  
2 voltammetric techniques exhibiting a linear sweep of the applied potential, its applicability  
3 breaks down when extended to pulse voltammetric techniques such as differential pulse  
4 voltammetry (DPV) and square-wave voltammetry (SWV). Pulse voltammetric techniques  
5 employ fundamentally different operating protocols, particularly in the potential modulations,  
6 and in the manner the current is sampled in each of the applied pulses [2,8-10]. These specific  
7 features, in turn, lead to significant deviations from the conditions under which the Randles-  
8 Sevcik equation holds. As it is already well elaborated elsewhere [2,8-10], in the pulse  
9 voltammetric technique, current is not measured continuously. Instead, it is sampled at specific  
10 time intervals, commonly at the end of each applied potential pulse. The aim of such a current-  
11 measuring protocol in pulse voltammetric techniques is to efficiently discriminate the  
12 capacitive (non-Faradaic) current [2,9,10]. Upon application of each potential pulse in pulse  
13 voltammetric techniques, perturbations of the electrochemical double layer induce distortions  
14 of the diffusional profile of the redox species of interest [10]. As a result, the diffusion layer  
15 does not evolve in a continuous, linear fashion, as assumed in linear scan voltammetry. Instead,  
16 the diffusion profile is periodically disrupted and re-created with each applied potential pulse.  
17 Such a repeated perturbation of the diffusion layer profile in pulse voltammetric techniques  
18 introduces a level of complexity that renders the direct application of the Randles-Sevcik  
19 formalism. Notably, in pulse voltammetric techniques, the peak current becomes a complex  
20 function of all signal parameters associated with the applied potential excitation waveform. In  
21 SWV, for example, the measured current depends on all parameters of the applied potential  
22 signal, i.e., the SW frequency, the SW pulse amplitude, and the potential step of the applied  
23 square-wave pulses [9]. In the voltammetric experiments, these parameters significantly affect  
24 the effective thickness of the diffusion layer, often resulting in complex voltammetric responses  
25 in which peak currents exhibit a nonlinear dependence on the applied signal parameters [9, 10].  
26 Consequently, the interpretation of peak current dependencies in pulse voltammetric  
27 techniques requires alternative models that explicitly account for the transient nature of mass  
28 transport and the dynamic reconfiguration of the interfacial region during each applied  
29 potential pulse. The non-steady-state conditions, altered diffusion dynamics, and distinct  
30 measurement protocols inherent to these methods necessitate a fundamentally different  
31 analytical framework for accurate data interpretation, which has not been developed so far.  
32 Thus, while the Randles-Sevcik equation remains a cornerstone in linear scan voltammetric  
33 analysis, its assumptions are not completely met in pulse voltammetric techniques. In this  
34 study, we present a set of theoretical results aimed at elucidating the limitations of applying  
35 Randles-Sevcik-like equations to describe the peak current dependences in square-wave  
36 voltammetry. Furthermore, we identify and discuss the key parameters that govern the  
37 magnitudes of peak current responses and influence the apparent reversibility of redox  
38 processes under square-wave voltammetric conditions. The analyses presented in this work

1 provide a foundational basis for the development of more comprehensive theoretical models,  
2 ultimately enabling the formulation of analytical expressions describing peak current  
3 dependencies in square-wave voltammetry.

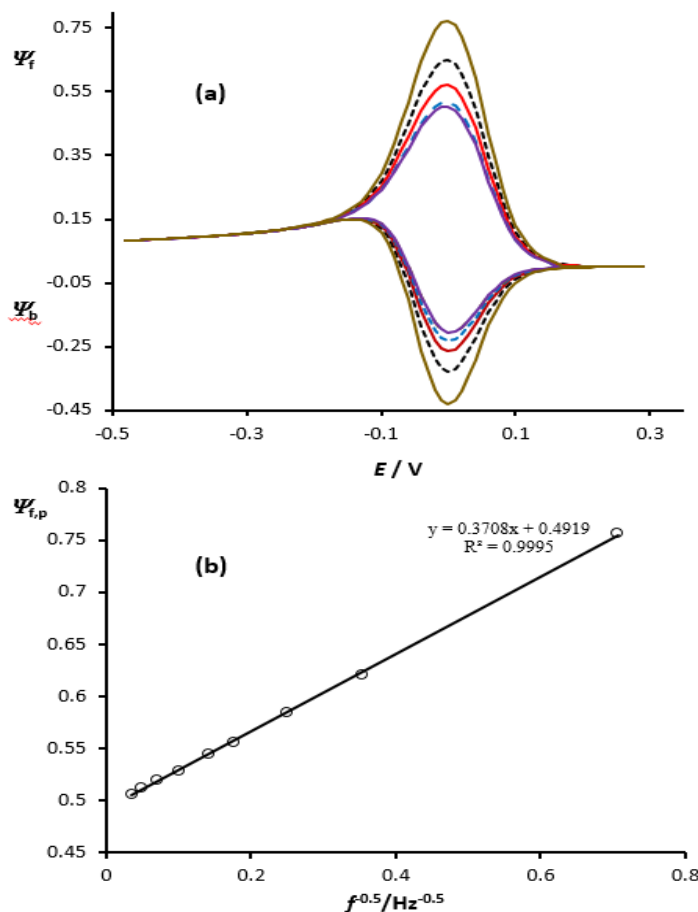
## 4 5 **2. MATHEMATICAL MODEL**

6 In this study, a theoretical model of a “Nernstian” (electrochemically reversible), diffusion-  
7 controlled electrode reaction of the type  $\text{Ox} + 1\text{e}^- \rightleftharpoons \text{Red}$  was investigated under conditions of  
8 square-wave voltammetry. The simulation protocol employed follows the methodology  
9 outlined in [9]. Square-wave voltammograms were calculated by using the MATHCAD  
10 commercial software package, implementing the algorithm described in more detail in [11].

## 11 12 **3. RESULTS AND DISCUSSION**

### 13 **3.1. The effect of square-wave frequency and the “effective scan rate” in square-wave** 14 **voltammetry**

15 Theoretical square-wave voltammograms of a simple one-electron, diffusion-controlled  
16 reversible Nernstian electrode reaction exhibit almost symmetrical forward and backward  
17 current peaks, centered around the formal potential ( $E^\circ$ ) (Figure 1a). As elaborated in [9], the  
18 features of theoretical SW voltammograms are primarily governed by the square-wave  
19 amplitude ( $E_{\text{sw}}$ ), step potential ( $dE$ ), frequency ( $f$ ), temperature ( $T$ ), and the diffusion  
20 coefficient ( $D$ ) of the electroactive species. The peak shape and intensity of both SW peaks are  
21 highly sensitive to these factors. Under constant temperature, step potential, and amplitude, the  
22 dimensionless peak currents are inversely proportional to the square root of the product of  
23 frequency and diffusion coefficient. For a given magnitude of  $D$ , the parameter  $(D \times f)^{0.5}$   
24 reflects the reduced diffusion time at higher frequencies, which limits the development of  
25 concentration gradients and thus lowers the peak currents [9]. Consequently, increasing  
26 frequency commonly results in diminished current responses of theoretical dimensionless SW  
27 peak currents. Importantly, for an ideal Nernstian redox system, the peak-to-peak separation  
28 between forward and backward currents remains constant, even at very high frequencies, while  
29 the peak current ratio (oxidation/reduction) remains unity across all frequencies applied. These  
30 criteria are commonly used to define the term “electrochemical reversibility” under the  
31 conditions of square-wave voltammetry [9]. All these features are nicely demonstrated in  
32 Figure 1a, where the behavior of forward and backward voltammetric profiles is evaluated as  
33 a function of applied frequency, while Figure 1b showcases the forward peak currents plotted  
34 vs.  $f^{0.5}$ . In square-wave voltammetry, however, instead of interpreting the results in light of the  
35 effect of frequency, one often (especially by commercial potentiostats producers) explores the  
36 term “effective scan rate” [12].



1

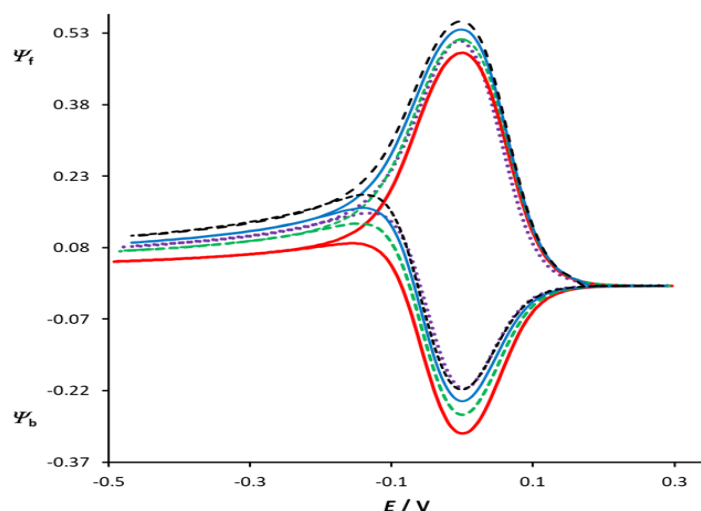
2 **Figure 1. (a)** Forward and backward components of the square-wave voltammograms plotted  
 3 as a function of the applied square-wave frequencies. **(b)** Graph of the dependence of the  
 4 forward peak current as a function of the inverse square root of the applied frequencies. In all  
 5 simulations, the initial potential was fixed at + 0.3 V, while the other calculation parameters  
 6 were: temperature  $T = 298.15$  K, potential step  $dE = 4$  mV, and square-wave amplitude  $E_{sw} =$   
 7 50 mV

8

9 The effective scan rate in SWV is commonly defined as  $\nu = dE \times f$ . This parameter is  
 10 commonly seen as an indicator that shows how rapidly the potential is swept through the redox  
 11 region upon applying a single potential SW pulse. In general context, the effective scan rate is  
 12 crucial parameter used to assess the balance between kinetics of electron transfer and the rate  
 13 of mass transport. Understanding this parameter helps in interpreting how experimental  
 14 conditions affect peak shapes, peak position, and the peak current magnitude. Shown in Figure  
 15 2 is a series of voltammetric patterns, calculated at identical “effective scan rates” that are  
 16 obtained for different combinations of  $dE$  and  $f$ . The potential step, defined as the increment  
 17 between successive potential pulses in square-wave voltammetry (SWV) [9], plays a critical  
 18 role in shaping the resulting voltammetric response. As the potential step increases, the  
 19 calculated voltammogram covers a broader potential range in a shorter number of pulses, thus

1 leading to broader and more pronounced peak features. This enlargement of the peaks at higher  
2 potential step magnitudes arises due to the greater driving force for electron transfer, which  
3 enhances the overall current response, while reducing the same time resolution of current-  
4 potential response by merging closely spaced redox events. Note that in all patterns in Figure  
5 2, the effective scan rate is the same, but this parameter is achieved by different combinations  
6 of the magnitude of the potential step and that of the applied square-wave frequency. Notably,  
7 the effective scan rate does not cause a shift of the positions of both peaks, indicating that peak  
8 potentials are predominantly governed by the thermodynamics of the redox process. However,  
9 the ratio between the forward and backward peak currents shows a subtle dependence on the  
10 effective scan rate, despite the fact that the nominal scan rate remains constant across all  
11 voltammetric patterns displayed in Figure 2. This behavior likely arises from some  
12 asymmetries in mass transport dynamics that become more pronounced under faster  
13 perturbation conditions. The behavior of square-wave voltammograms displayed in Figure 2  
14 underscores the importance of potential step and the SW frequency (i.e. the effective scan rate)  
15 in terms of better quantitative interpretation of peak-current dependences in SWV.

16



17

18 **Figure 2.** Forward and backward current components of square-wave voltammograms  
19 simulated at an "effective" scan rate of 200 mV/s, achieved by various combinations of  
20 potential step ( $dE$ ) and frequency ( $f$ ):  $dE = 2$  mV,  $f = 100$  Hz (.....);  $dE = 4$  mV,  $f = 50$  Hz  
21 (—);  $dE = 5$  mV,  $f = 40$  Hz (-----);  $dE = 8$  mV,  $f = 25$  Hz (—); and  $dE = 10$  mV,  $f = 20$   
22 Hz (-----). All other simulation parameters were identical to those reported in Figure 1.

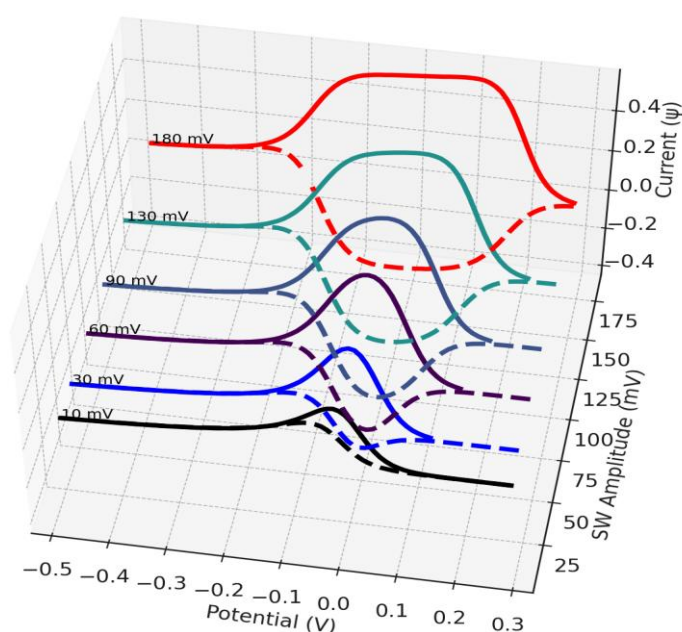
23

### 24 3.2. Effect of the square-wave amplitude

25 It is already reported [9,10,13,14], that the application of each potential pulse in pulse  
26 voltammetric techniques perturbs the electrochemical double thereby altering the concentration

1 gradients of the redox species within the diffusion layer [15-17]. Unlike linear scan  
2 voltammetry, where the diffusion layer evolves gradually and predictably [2-4], SWV imposes  
3 periodic interruptions to this development [9]. Application of each successive potential SW  
4 pulse induces a transient reorganization of the diffusion profile, thus preventing a steady-state  
5 or linear progression within. These repeated disturbances create complex and time-dependent  
6 concentration profiles of redox-active species of interest that must be considered when  
7 interpreting the current-potential responses in SWV [9,11]. It is particularly important to note  
8 that the amplitude of the square-wave pulses plays a critical role in modulating this complexity,  
9 as it governs the interplay between the thermodynamic driving force and the extent of  
10 diffusion-layer evolution [18]. Therefore, it is of utmost importance to this study to understand  
11 the effect of square-wave amplitude on the development of square-wave voltammetric patterns.  
12 Shown in Figure 3 is a series of 3-D voltammetric patterns (forward and backward current  
13 components), calculated at different SW amplitudes. The absence of a backward peak in  
14 theoretical voltammograms calculated at low square-wave amplitudes (at  $E_{sw}$  of 10 mV or  
15 lower) is due to the insufficient overpotential to significantly drive the reverse (oxidation)  
16 reaction within the short pulse time.

17



18

19 **Figure 3.** Forward and backward 3D current profiles of square-wave voltammograms  
20 simulated at varying square-wave amplitudes. A fixed frequency of 50 Hz was applied for all  
21 calculations, while all other simulation parameters were identical to those reported in Figure 1.

22

23 At low amplitudes, the potential excursions are close to the formal potential ( $E^{\ominus}$ ), where the  
24 system remains near equilibrium. In such a scenario, it is more likely that the same electrode  
25 transformation that takes place in the forward scan also happens in the backward scan. This

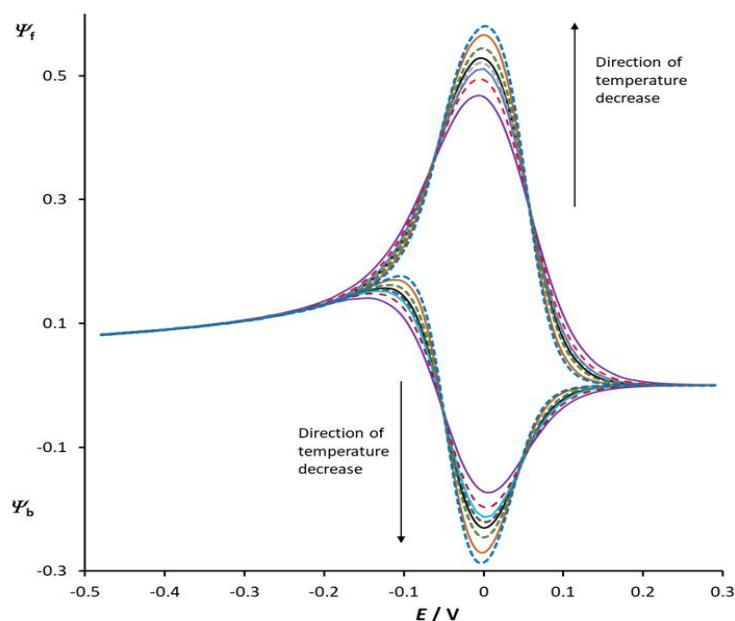
1 results in minimal driving force for the backward electron transfer during the reverse pulse,  
2 leading to small backward currents and the absence of a distinct backward peak. Essentially,  
3 the redox reaction does not proceed far enough in either direction to generate a noticeable  
4 reverse signal. So, when square-wave amplitudes exceed approximately 30 mV, the backward  
5 current components of the square-wave voltammograms begin to develop noticeably. This is  
6 because the increased amplitude provides a suitable overpotential, which drives the redox  
7 reaction further enough from equilibrium during each applied pulse. At these overpotentials,  
8 the electron transfer becomes more extensive, and sufficient time exists within each potential  
9 pulse for a concentration gradient to begin forming in the diffusion layer. This gradient enables  
10 both oxidation and reduction processes to generate measurable currents in forward and  
11 backward directions, leading to the appearance of distinct backward peaks in the  
12 voltammogram. On the other hand, at rather high square-wave amplitudes (e.g., at  $E_{sw} > 90$   
13 mV), both forward and backward current components tend to form broad plateaus rather than  
14 sharp or normally developed peaks. This occurs because the large potential excursions (e.g.,  $\pm$   
15 100 mV or higher) drive the system far from the equilibrium potential. The fast potential jumps  
16 cause rapid and nearly complete oxidation and reduction during each half-cycle of the square  
17 wave, so the surface concentration in the diffusional layer of the electroactive species is quickly  
18 depleted. As a result, the current becomes diffusion-limited almost immediately, and there is  
19 no time to re-establish a concentration gradient of redox-active species between applied pulses.  
20 Therefore, the current response at large SW amplitudes gets plateau-shaped features rather than  
21 the common peak-shaped. Any further increases in pulse amplitude do not contribute to the  
22 increase of peak currents. This behavior contrasts with the linear or quasi-linear increase in  
23 peak current observed at moderate amplitudes (e.g., 30–90 mV), where diffusion still governs  
24 the response. This plateauing of peak current at large square-wave amplitudes highlights one  
25 of the key limitations in applying Randles–Sevcik-type relationships to square-wave  
26 voltammetry. Since the current response under these conditions is no longer governed by linear  
27 diffusion but is instead constrained by the inability of concentration gradients to form within  
28 the short pulse duration, the major assumptions underlying the Randles–Sevcik equation break  
29 down.

30

### 31 **3.3. Effect of the temperature on the features of calculated square-wave voltammograms**

32 The effect of the temperature on the behavior of theoretical square-wave voltammograms  
33 of surface-active redox systems obeying Butler-Volmer formalism is elaborated in more detail  
34 elsewhere [19]. In voltammetric simulations, temperature is a parameter incorporated within  
35 the potential-dependent term of the Nernst equation, thereby influencing all features of the  
36 calculated square-wave voltammograms.

37

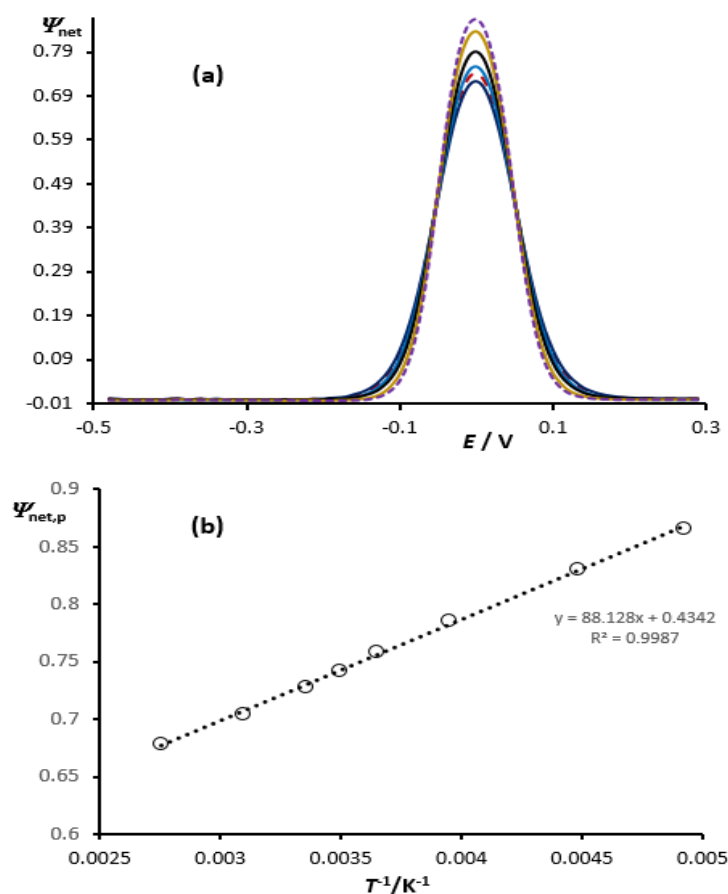


1  
2 **Figure 4.** Evolution of forward and backward current components of square-wave  
3 voltammograms as a function of temperature. Simulations were performed at temperatures  $T =$   
4 203, 223, 253, 274, 286, 298, 323, and 363 K, with the curves corresponding to increasing  
5 temperatures showing progressively lower current intensities. The simulation conditions  
6 included a frequency of 50 Hz, a square-wave amplitude of 60 mV, and a potential step of 10  
7 mV.

8  
9 As shown in Figure 4, decreasing the temperature leads to a notable increase in the peak  
10 currents of both oxidation and reduction processes. Simultaneously, the voltammetric peaks  
11 become sharper and more narrowly defined, the peak-to-peak separation diminishes, while the  
12 overall symmetry between the forward and backward peaks becomes more pronounced. The  
13 development of the net SW peaks as a function of the temperature, and the dependence between  
14 the net SW peaks and the inverse temperature are displayed in Figure 5a and 5b, respectively.  
15 Notably, the magnitudes of net SW peaks follow a linear dependence as a function of inverse  
16 temperature in the region of applied temperatures. The influence of temperature on the  
17 development of square-wave voltammograms becomes particularly evident when analyzing  
18 voltammograms calculated at small pulse amplitudes. Shown in Figure 6 is a series of 3D  
19 voltammograms calculated at SW amplitude of 25 mV, where the effect of temperature is  
20 displayed. The 3D visualization of square-wave voltammograms recorded at an amplitude of  
21 25 mV clearly demonstrates the significant influence of temperature on the electrochemical  
22 behavior of the considered diffusion-controlled Nernstian electrode mechanism. As the  
23 temperature decreases, a marked increase in the peak intensities is observed for both the  
24 forward and backward currents. At lower temperatures, the backward currents become more

1 pronounced and start to mirror their forward counterparts more closely, thus indicating an  
2 improvement in the overall apparent electrochemical reversibility.

3



4

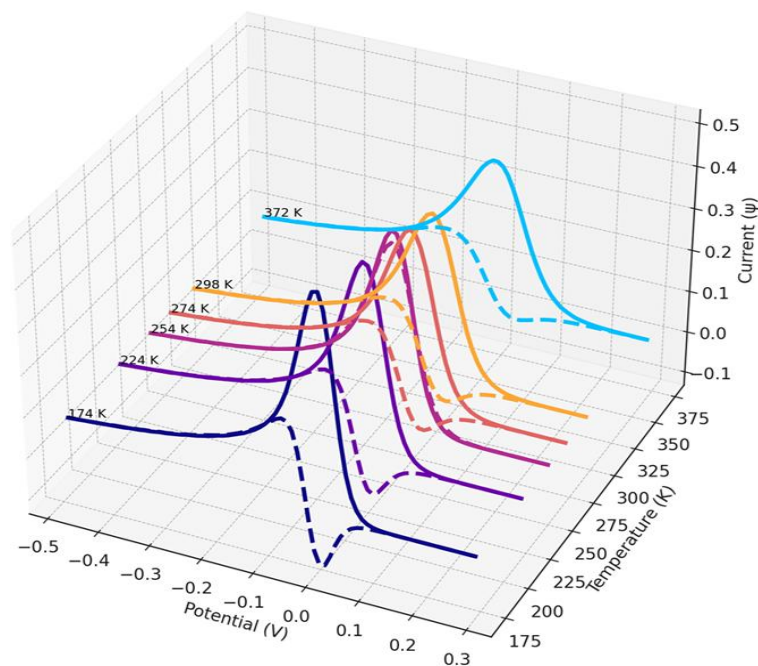
5 **Figure 5.** (a) Evolution of calculated net square-wave voltammograms as a function of  
6 temperature, and (b) the corresponding dependence of net peak currents on the inverse of  
7 thermodynamic temperature ( $1/T$ ). All simulation parameters were identical to those used in  
8 Figure 4.

9

10 The symmetry between the forward and backward peaks becomes more evident, especially  
11 at the lowest temperatures examined, implying that temperature exerts a critical role in  
12 modulating both the intensity and reversibility of square-wave voltammetric responses. The  
13 behavior of calculated voltammetric patterns presented in Figures 4, 5, and 6 arises from the  
14 temperature-dependent nature of the thermodynamic term governing concentration gradients  
15 near the electrode surface. At lower temperatures, the distribution of redox states around the  
16 formal potential narrows, which in turn leads to more abrupt changes in current near the redox  
17 potential. However, it is important to note that in real experimental conditions, the diffusion  
18 coefficients of electroactive species are also temperature-dependent parameters, typically  
19 decreasing by lowering the temperature [2,3], which introduces an additional level of  
20 complexity in experimental scenarios. As a result, experimentally observed peak currents may

1 not follow the same trends as those predicted by idealized simulations, where diffusion  
2 coefficients are held constant (as has been done in Figures 4 to 6 in this work).

3



4

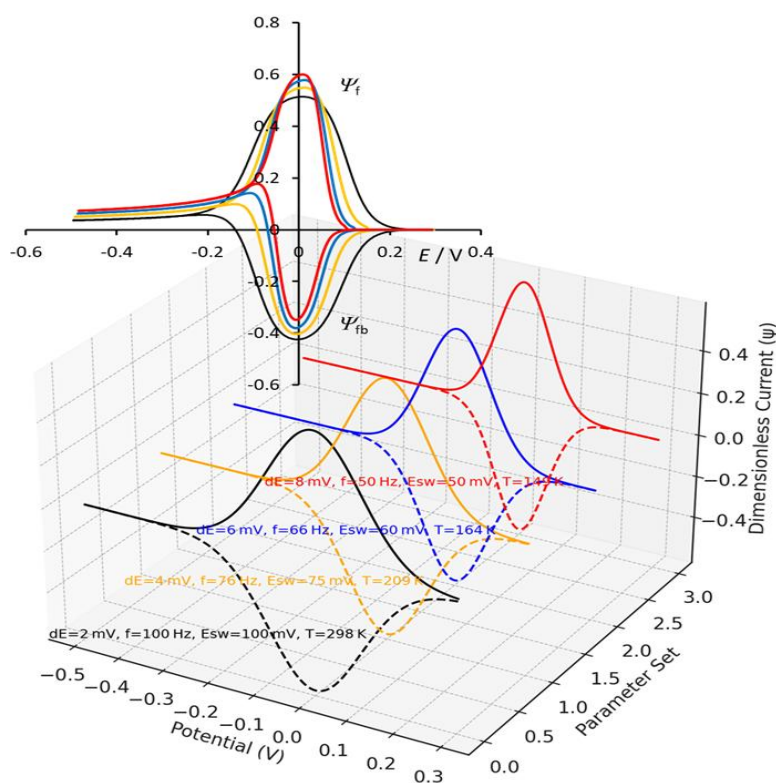
5 **Figure 6.** Three-dimensional profiles illustrating the effect of temperature on the evolution of  
6 forward and backward current components of square-wave voltammograms, simulated at a low  
7 square-wave amplitude of 25 mV. All other simulation parameters were identical to those  
8 described in Figure 4.

9

10 **3.4. If the Randles-Sevcik formalism is not applicable to SWV, is there any parameter**  
11 **that governs the peak current magnitudes in square-wave voltammetry?**

12 As shown in previous segments of this work, the Randles–Sevcik equation, traditionally  
13 used to describe peak currents in linear scan voltammetry under diffusion control, is not  
14 completely applicable for predicting peak currents in square-wave voltammetry. This  
15 limitation arises from the complex interplay of experimental parameters, such as the square-  
16 wave amplitude, potential step, frequency, and temperature, all of which collectively shape the  
17 structure of the diffusion layer and the concentration profile of the redox-active species of  
18 interest. Unlike linear scan voltammetry, where the concentration gradients evolve in a  
19 relatively predictable manner, square-wave voltammetry involves rapid potential modulation  
20 that disrupts the classical development of concentration profiles. Consequently, the  
21 voltammetric outputs become highly dependent on the dynamic and non-linear interactions  
22 between these parameters commonly arise. This makes the application of Randles–Sevcik  
23 formalism insufficient to fully describe the behavior of SWV peak currents under diffusional  
24 conditions. In practice, the temperature-dependent nature of the diffusion coefficient introduces

1 additional variability that the Randles–Sevcik framework cannot accommodate. As evidenced  
 2 in Figures 2 through 6, the peak currents might exhibit a non-trivial dependence on potential  
 3 step, frequency, temperature, and square-wave amplitude, indicating that no single analytical  
 4 expression like the Randles–Sevcik equation can universally describe the system. Therefore, a  
 5 semi-empirical approach remains the most viable strategy to determine which parameters  
 6 predominantly govern the peak current in SWV, in agreement with the observed experimental  
 7 trends.  
 8



9

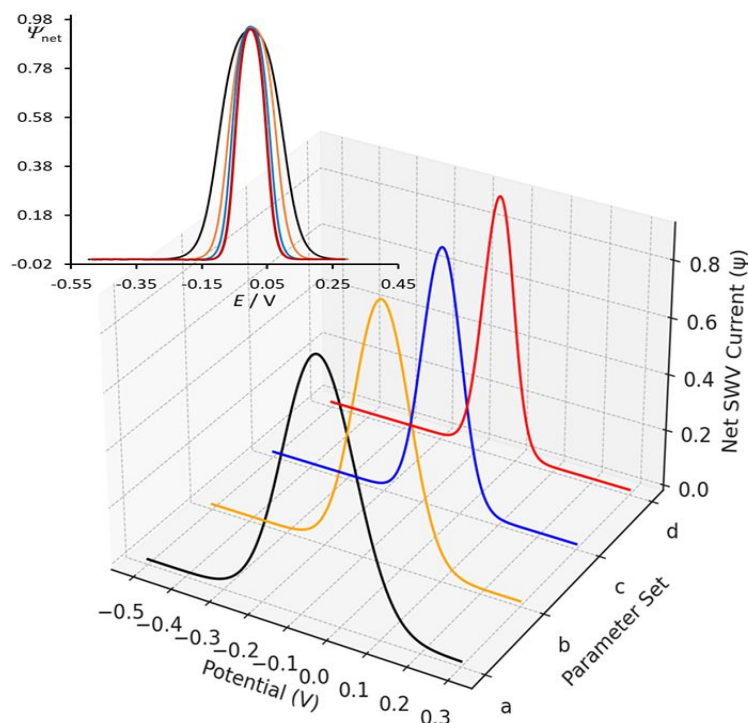
10 **Figure 7.** Three-dimensional voltammetric profiles of the forward and backward current  
 11 components, illustrating their evolution as a function of a unified parameter  $\chi/const. = 27.528$ ,  
 12 which incorporates the effects of potential step ( $dE$ ), frequency ( $f$ ), square-wave amplitude  
 13 ( $E_{sw}$ ), and temperature ( $T$ ). The parameter  $\chi$  is defined as  $\chi = const. \cdot (F/RT) \cdot [E_{sw}/(dE \cdot f)]^{1/2}$ . The  
 14 combinations of  $dE$ ,  $f$ ,  $E_{sw}$  and  $T$  unified in parameter  $\chi/const. = 27.528$  are given in the 3D  
 15 graph next to each corresponding voltammogram. In the left upper corner, 2D graph of forward  
 16 and backward current components of voltammograms simulated for  $\chi/const. = 27.528$   
 17 corresponding to the conditions given in the 3D plot are shown.

18

19 The analysis of square-wave voltammograms presented in Figure 7 reveals a compelling  
 20 observation: despite the variation of fundamental experimental parameters such as step  
 21 potential ( $dE$ ), square-wave amplitude ( $E_{sw}$ ), frequency ( $f$ ), and temperature ( $T$ ), the symmetry  
 22 and magnitude of the forward and backward current components remain remarkably consistent

1 when a specific composite parameter is held constant. This dimensionless parameter, defined  
 2 as  $\chi = \text{const.} \cdot (F/RT) \cdot [E_{\text{sw}}/(dE \cdot f)]^{1/2}$ , effectively governs the peak currents of a voltammetric  
 3 response under Nernstian conditions.

4



5

6 **Figure 8.** Three-dimensional net square-wave voltammetric profiles corresponding to the  
 7 voltammetric patterns presented in Figure 7. In the left upper corner, 2-D graph of net SW  
 8 current components of voltammograms simulated for magnitude of parameter  $\chi/\text{const.} = 27.528$   
 9 corresponding to the conditions given in the 3-D plot are displayed.

10

11 In the last equation,  $F$  is the Faraday constant, while  $R$  is the universal gas constant. The  
 12 voltammograms calculated at different sets of  $(dE, f, E_{\text{sw}}, T)$  but constant  $\chi$  value ( $\chi/\text{const.} =$   
 13  $27.528$  in the current set of calculations at Figure 7) exhibit nearly identical ratios between  
 14 forward and backward peak currents (Figure 7), with net SW peak currents also showing  
 15 minimal variation (Figure 8). The numerical values of the forward, backward, and net peak  
 16 currents calculated under varying experimental conditions, specifically different values of step  
 17 potential, square-wave amplitude, frequency, and temperature, are summarized in Table 1.

18 Importantly, despite these variations in magnitudes of  $dE, f, E_{\text{sw}}, T$ , all simulations were  
 19 performed at a constant value of the composite parameter  $\chi/\text{const.} = 27.528$ . The data presented  
 20 in Table 1 clearly demonstrate that the  $\chi$  parameter exerts a significant and consistent influence  
 21 on the resulting voltammetric peak currents. The near-identical magnitudes of both forward  
 22 and backward components, as well as the net peak currents across all experimental sets,  
 23 underscore the critical role of  $\chi$  in governing the magnitudes of peak currents of theoretical  
 24 square-wave voltammetric responses.

1 **Table 1.** Relevant features of simulated SW voltammograms, calculated at constant parameter  
 2  $\chi/\text{const.} = (F/RT) \cdot [E_{\text{sw}}/(dE \cdot f)]^{1/2} = 27.528$ . Magnitude of  $\chi/\text{const.} = 27.528$  is obtained via  
 3 different combinations of  $dE$ ,  $f$ ,  $E_{\text{sw}}$  and  $T$  (magnitudes of peak currents obtained with the  
 4 tangent method)

Parameter $\chi/\text{const.} = (F/RT) \cdot [E_{\text{sw}}/(dE \cdot f)]^{1/2} = 27.528$ in all cases, obtained from combination of following simulation parameters	Magnitude of forward (reduction) peak current $\Psi_{f,p}$	Magnitude of backward (oxidation) peak current $\Psi_{b,p}$	Magnitude of net SWV peak current $\Psi_{\text{net,p}}$
<b>Black curve:</b> $dE = 2 \text{ mV}$ , $f = 100 \text{ Hz}$ , effective scan rate = 200 mV/s $E_{\text{sw}} = 100 \text{ mV}$ , $T = 298 \text{ K}$	0.458	-0.457	0.915
<b>Orange curve:</b> $dE = 4 \text{ mV}$ , $f = 76 \text{ Hz}$ , effective scan rate = 304 mV/s $E_{\text{sw}} = 75 \text{ mV}$ , $T = 209 \text{ K}$	0.460	-0.458	0.918
<b>Blue curve:</b> $dE = 6 \text{ mV}$ , $f = 66 \text{ Hz}$ , effective scan rate = 396 mV/s $E_{\text{sw}} = 60 \text{ mV}$ , $T = 164 \text{ K}$	0.460	-0.460	0.920
<b>Red curve:</b> $dE = 8 \text{ mV}$ , $f = 50 \text{ Hz}$ , effective scan rate = 400 mV/s $E_{\text{sw}} = 50 \text{ mV}$ , $T = 149 \text{ K}$	0.462	-0.463	0.925

5

6 **4. CONCLUSION**

7 As shown in previous segments of this work, the Randles–Sevcik equation, traditionally  
 8 used to describe peak currents dependence in linear scan voltammetry for Nernstian redox  
 9 systems under diffusion control, is not completely applicable for predicting peak currents in  
 10 square-wave voltammetry. This limitation arises from the complex interplay of experimental  
 11 parameters, such as the square-wave amplitude, potential step, frequency, and temperature, all  
 12 of which collectively shape the structure of the diffusion layer, and so the concentration profile  
 13 of the redox-active species. Unlike linear scan voltammetry, where the concentration gradients  
 14 evolve in a relatively predictable manner, square-wave voltammetry involves rapid potential  
 15 modulation that disrupts the classical development of concentration profiles in diffusion layer.  
 16 Consequently, the voltammetric outputs become highly dependent on the dynamic and  
 17 complex interactions between these parameters. This makes the application of Randles-Sevcik  
 18 formalism insufficient to fully describe the behavior of SWV peak currents under diffusional  
 19 conditions. Large applied SW amplitudes (larger than 100 mV), and large potential steps (larger  
 20 than 10 mV) commonly cause huge disruptions of the applied potential. This will generate  
 21 driving forces that make the redox process to proceed very rapidly. The flattened voltammetric  
 22 responses and the suppression of well-defined peak formation at large applied SW amplitudes

1 are attributed to the insufficient development of diffusional concentration gradients within the  
2 time frame of the applied potential pulses. These effects highlight the major limitations of  
3 applying the Randles–Sevcik formalism under square-wave voltammetric conditions, where  
4 the transient and pulsed nature of the technique, coupled with temperature dependences on all  
5 voltammetric features, precludes the use of simplified linear diffusion-based models. However,  
6 the major results evaluated in this work suggest that a complex parameter  $\chi$ , defined as  $\chi =$   
7  $const. \cdot (F/RT) \cdot [E_{sw}/(dE \cdot f)]^{1/2}$ , functions as a key parameter that largely defines the peak currents  
8 of SW voltammetric peaks, despite wide variations in input conditions. This behavior holds for  
9  $E_{sw}$  in the range of 40 mV and 100 mV, and  $dE$  between 2mV and 10 mV, indicating the  
10 robustness of parameter  $\chi$  in defining crucial role across a broad practical domain. This finding  
11 opens a new perspective for modeling in square-wave voltammetry and suggests that the  $\chi$   
12 parameter (which may be referred to as the “JPG” parameter, named after the initials of Janeva,  
13 Kokoskarova, and Gulaboski) may serve, under SWV conditions, as an analog to the Randles–  
14 Sevcik function in linear scan voltammetry. In practice, however, the temperature dependence  
15 of the diffusion coefficient introduces additional complexity that falls outside the predictive  
16 capacity of the Randles-Sevcik framework. Therefore, this parameter  $\chi$  reflects a slight  
17 dependence of the diffusion coefficient on temperature, consistent with real experiments  
18 typically conducted in the range of 285–300 K [20]. Nevertheless, the findings presented in  
19 this work may serve as an initial step towards forming a theoretical basis for developing a  
20 generalized predictive equation that relates peak currents to measurable parameters under  
21 square-wave modulation. Such a parameter-driven approach could significantly facilitate the  
22 rational design, interpretation, and standardization of SWV experiments in applied  
23 electroanalysis. In our subsequent model, this approach will be applied to identify the  
24 governing parameter for square-wave voltammetric peak currents in more complex kinetic  
25 systems, as described within the framework of the Butler-Volmer formalism.

26

## 27 **Acknowledgments**

28 Rubin Gulaboski thanks the Alexander von Humboldt Foundation (Germany) for the  
29 support via project with Ref 3.4-1070534-MKD-IP. All authors of this work would like to  
30 thank the “Goce Delcev” University, Stip, Macedonia, for the permanent support.

31

## 32 **Declarations of interest**

33 The authors declare no conflict of interest in this reported work.

34

## 35 **REFERENCES**

- 36 [1] F.A. Armstrong, in: A.J. Bard, M. Stratmann, and G.S. Wilson (Eds.), Encyclopedia of  
37 Electrochemistry, Wiley-VCH, Weinheim (2020).

- 1 [2] J.M. Saveant, and C. Costent, Elements of Molecular and Biomolecular  
2 Electrochemistry: An Electrochemical Approach to Electron-Transfer Chemistry, 2<sup>nd</sup> ed.,  
3 John Wiley & Sons (2019).
- 4 [3] R.G. Compton, and C. E. Banks, Understanding Voltammetry, 2<sup>nd</sup> ed. Imperial College  
5 Press, London, 2011.
- 6 [4] N. Elgrashi, K.J. Rountree, B.D. McCarthy, E.S. Rountree, T.T. Eisenhart, and J. L.  
7 Dempsey, J. Chem. Educ. 95 (2018) 197.
- 8 [5] G.A. Mabbott, J. Chem. Educ. 60 (1983) 697.
- 9 [6] P.T. Kissinger, and W.R. Heineman, J. Chem. Educ. 6 (1983) 702.
- 10 [7] A. Sevcik, Collect. Czech. Chem. Commun. 13 (1948) 349.
- 11 [8] A.J. Bard and R.A. Faulkner, Electrochemical methods: Fundamentals and applications,  
12 2<sup>nd</sup> ed, Wiley, New York (2011).
- 13 [9] V. Mirceski, S. Komorsky-Lovric, and M. Lovric, in: F. Scholz (Ed.), Square-Wave  
14 Voltammetry, Theory and Application, Springer, Berlin (2007).
- 15 [10] A. Molina, and J. Gonzalez, Pulse voltammetry in physical chemistry and electroanalysis:  
16 Theory and applications, F. Scholz, ed. Springer, Germany (2016).
- 17 [11] R. Gulaboski, and V. Mirceski, J. Solid State Electrochem. 28 (2024) 1121.
- 18 [12] Gamry Instruments. Square-Wave Voltammetry, Gamry Application Notes (2018).
- 19 [13] A. Molina, J. Gonzalez, F. Martinez-Ortiz, and R. G. Compton, Geometrical insights of  
20 Transient Diffusion Layers, J. Phys. Chem. C 114 (2010) 4093.
- 21 [14] J. V. Hernandez Tovar, A. J. Martinez-Garcia, M. Lopez-Tenes, F. Martinez-Ortiz, A.  
22 Molina, and J. Gonzalez, Anal. Chem. 97 (2025) 2941.
- 23 [15] J.L. Melville, and R.G. Compton, Electroanalysis 13 (2001) 123.
- 24 [16] A. Molina, E. Laborda, F. Martínez-Ortiz, D.F. Bradley, D.J. Schiffrin, and R.G.  
25 Compton, J. Electroanal. Chem. 659 (2011) 12.
- 26 [17] E. Laborda, J. Gonzalez, and A. Molina, Electrochem. Commun. 43 (2014) 25.
- 27 [18] A.A. Sher, A.M. Bond, D.J. Gavaghan, K. Gillow, N.W. Duffy, S. Guo, and J.  
28 Zhang, Electroanalysis, 17 (2005) 1450.
- 29 [19] R. Gulaboski, M. Lovric, V. Mirceski, I. Bogeski, and M. Hoth, Biophys. Chem. 137  
30 (2008) 49.
- 31 [20] R.A. Meyers, Encyclopedia of Physical Science and Technology, 3<sup>rd</sup> edition (2001)  
32 Elsevier.